Msh homeobox 1 (*Msx1*)- and *Msx2*-overexpressing bone marrow-derived mesenchymal stem cells resemble blastema cells and enhance regeneration in mice

Received for publication, December 28, 2016, and in revised form, April 29, 2017 Published, Papers in Press, May 1, 2017, DOI 10.1074/jbc.M116.774265

Leila Taghiyar[‡§], Mahdi Hesaraki[‡], Forough Azam Sayahpour[‡], Leila Satarian[‡], Samaneh Hosseini[‡], Naser Aghdami[‡], and Mohamadreza Baghaban Eslaminejad[‡1]

From the [‡]Department of Stem Cells and Developmental Biology, Cell Science Research Center, Royan Institute for Stem Cell Biology and Technology, Academic Center for Education, Culture and Research (ACECR), Tehran 1665659911, Iran and the [§]Department of Developmental Biology, University of Science and Culture, Tehran 13145-871, Iran

Edited by Xiao-Fan Wang

Amputation of the proximal region in mammals is not followed by regeneration because blastema cells (BCs) and expression of regenerative genes, such as Msh homeobox (*Msx*) genes, are absent in this animal group. The lack of BCs and positional information in other cells is therefore the main obstacle to therapeutic approaches for limb regeneration. Hence, this study aimed to create blastema-like cells (BlCs) by overexpressing *Msx1* and *Msx2* genes in mouse bone marrow-derived mesenchymal stem cells (mBMSCs) to regenerate a proximally amputated digit tip. We transduced mBMSCs with *Msx1* and *Msx2* genes and compared osteogenic activity and expression levels of several *Msx*-regulated genes (*Bmp4*, *Fgf8*, and keratin 14 (*K14*)) in BlC groups, including MSX1, MSX2, and MSX1/2 (in a 1:1 ratio) with those in mBMSCs and BCs *in vitro* and *in vivo* following injection into the amputation site. We found that *Msx* gene overexpression increased expression of specific blastemal markers and enhanced the proliferation rate and osteogenesis of BlCs compared with mBMSCs and BCs via activation of *Fgf8* and *Bmp4*. Histological analyses indicated full regrowth of digit tips in the *Msx*-overexpressing groups, particularly in MSX1/2, through endochondral ossification 6 weeks post-injection. In contrast, mBMSCs and BCs formed abnormal bone and nail. Full digit tip was regenerated only in the MSX1/2 group and was related to boosted *Bmp4, Fgf8*, and *K14* gene expression and to limb-patterning properties resulting from *Msx1* and *Msx2* overexpression. We propose that *Msx*-transduced cells that can regenerate epithelial and mesenchymal tissues may potentially be utilized in limb regeneration.

Digit tip regeneration is a well-documented example of organ/appendage regeneration in lower vertebrates, such as salamanders, because they exhibit robust regeneration potential in response to amputation anywhere along the proximal/distal limb axis (1). However, the level of amputation through the terminal phalanx causes various regeneration responses in mammals, such as humans and mice. Amputation in the middle of the terminal phalanx involves complete skeletal restoration, whereas only scar formation occurs following amputation injury at the proximal level (2). Therefore, the main goal of clinical and experimental investigations is to restore lost parts of limbs damaged due to disease or injury. Despite numerous attempts, digit tip regrowth after amputation through terminal phalanges remains challenging. Naturally, blastema cells (BCs)[2] are considered a key mediator of digit tip regeneration so that their removal following proximal amputation leads to scar formation in adult mammals (1).

BCs are believed to be a heterogeneous population of lineage-restricted progenitor cells derived from fibroblasts of connective tissue (3). There are several main surface biomarkers assigned to BCs: stem cell antigen-1 (*Sca-1*), endothelial marker (CD31), and vimentin (4). Msh homeobox (*Msx*) genes are members of the *Hox* gene family and include 1 *Msx1* (*Hox7*) and *Msx2* (*Hox8*). They are highly conserved among vertebrates and are considered key genes in BCs (5, 6). It has conclusively been shown that the absence of BCs as well as *Msx1* and *Msx2* genes results in regeneration failure in a proximal amputation of adult mice (7). Additionally, *Msx* genes are of crucial importance in ecto-mesodermal interactions that mediate cellular proliferation and differentiation during limb formation, apical epithelial cap (AEC) formation, and limb patterning (8). Bensoussan-Trigano *et al.* (9) have shown that the Prx1-Cre *Msx1* null/null *Msx2* null/Flox mutants display abnormal digit formation and preaxial polydactyly in fetal mouse digit tip regeneration. Overexpressed *Msx1* (*Hox7*) in hind-limb regeneration in a transgenic *Xenopus* model (M1) resulted in a higher proliferation rate in both BCs and apical epithelial cap, thickened wound epithelium, and more regenerated toes in M1 compared with

The present research was supported by the Royan Institute and the Iranian Council of Stem Cell Research and Technology (ICSCR). The authors declare that they have no conflicts of interest with the contents of this article.
This article contains supplemental Tables 1 and 2 and Figs. 1–3.

[1] To whom correspondence should be addressed: Dept. of Stem Cells and Developmental Biology, Cell Science Research Center, Royan Institute for Stem Cell Biology and Technology, 1665659911, ACECR, Tehran, Iran. Tel.: 98-2123562524; Fax: 98-2123562507; E-mail: eslami@royaninstitute.org.

[2] The abbreviations used are: BC, blastema cell; BMSC, bone marrow-derived mesenchymal stem cell; mBMSC, mouse bone marrow-derived mesenchymal stem cell; BlC, blastema-like cell; MSC, mesenchymal stem cell; CFU-F, colony-forming unit fibroblast; ALP, alkaline phosphatase; MTT, 3-(4,5-dimethylthiazol-2-yl)-2,5-diphenyltetrazolium bromide; ICC, immunocytochemistry; Nrm. Reg, normal regeneration; Al & Al, Alcian blue and alizarin red S; WPI, weeks post-injection; DPA, days post-amputation; qRT-PCR, quantitative RT-PCR; IRES, internal ribosome entry site.

WT animals in stage 54 (10). More importantly, BCs have enabled the process of bone formation as a main process of limb regeneration by triggering a cascade-of-cell-signaling pathway, such as bone morphogenetic proteins (BMPs) and FGFs (11–13). Positional information is one of the key elements in successful regeneration. It has been proposed that the expression of region-specific *hox* genes in early and late blastema tissues is more likely to be related to positional identity (14). Rao *et al.* (15) have shown that fibroblastemas of *Xenopus* limbs express proximal-distal axial patterning genes, including *hoxa9*, *hoxa11*, and *hoxa13*. Indeed, successful limb regeneration has been correlated to the formation of BCs and their related genes. Although transplantation of BCs at the amputation site could accelerate wound healing and digit regeneration, availability of BCs has always been a challenging issue in terms of digit regeneration. Hence, the use of an alternative available cell source with high similarity to BCs would be a valuable strategy in limb regeneration.

Various cell sources have been isolated and characterized in terms of their potential in clinical settings. Fetal limb cells have a tremendous degree of similarity to BCs for limb regeneration, although their administration is hampered due to ethical concerns (16). Stem cells, in particular mesenchymal stem cells (MSCs), have tremendous potential in therapeutic approaches due to their unique characteristics of self-renewal and differentiation potential. MSCs are multipotent cells that exist in most adult tissues (17–19) and have the ability to give rise to multiple tissue-forming cell lineages (20–22). It has been postulated that MSCs affect cell migration, proliferation, and survival of the surrounding cells as well as providing anti-scarring properties through paracrine signaling (23, 24). They may also regulate immune and inflammatory responses, making them an appropriate therapeutic candidate for treating inflammatory diseases (25, 26). Thus far, much research has been devoted to the application of MSCs in various diseased tissues due to their potent regenerative capacity, and they have been used in over 350 clinical trials worldwide (27). However, there has been little investigation of MSCs in limb regeneration. Masaki *et al.* (28) transplanted bone marrow-derived MSCs (BMSCs) and limb buds into amputated limbs in neonatal mice and observed the generation of the segmented pattern of bone and cartilage. In another study, injection of the hematopoietic stem cells into an amputated digit did not lead to the formation of main structures of the digit, but it contributed to the formation of blood cells and bone marrow tissue (29). However, a lack of positional information in current efforts that use stem cells is more likely to be the cause of regeneration failure.

In our previous study, we isolated BCs from neonatal mice and compared their characteristics with mouse BMSCs (mBMSCs) *in vitro*. Our study has shown that mBMSCs have similar characteristics to BCs in terms of growth and osteogenic activity and can be considered as substitutes for BCs (30). Thus, the present study aimed to create blastema-like cells (BlCs) through overexpression of *Hox* family genes, including *Msx1* and *Msx2*, that are involved in positional information in mBMSCs and regenerate a digit tip by transplantation of BlCs *in vivo*. Therefore, we transduced mBMSCs with *Msx1* and *Msx2* genes, after which their proliferation and differentiation potentials were examined by 3-(4,5-dimethylthiazol-2-yl)-2,5-diphenyltetrazolium bromide (MTT) and real-time PCR *in vitro*. To determine the regenerative potential of BlCs, we injected them into the amputated proximal digits of adult mice. The results demonstrated that BlCs could completely improve proximal digit tip amputation compared with mBMSCs and BCs.

Results

Msx1- and Msx2-transduced mBMSCs

To verify the accuracy of gene transduction, third-generation self-inactivating vectors with various fluorescent reporters' genes were constructed as diagrammed in Fig. 1*A*. *Msx1* and *Msx2* genes were co-expressed by GFP and tdTomato genes, respectively. Although the majority of cells expressed reporter genes, we needed a pure cell population that absolutely expressed *Msx1* (GFP^+) and *Msx2* ($tdTomato^+$). Therefore, the cells were sorted for GFP and tdTomato markers after 72 h of transduction, as seen in Fig. 1*B* (*a* and *b*). ICC analysis showed significantly lower protein expression levels of endogenous *Msx1* and *Msx2* in mBMSCs (< 3–5%) compared with BCs (30–40%). *Msx1* and *Msx2* transduction led to a drastic increase in expression level of these exogenous genes in BlCs (100%), which was greater than in BCs (Fig. 1*C*, *a* and *c*).

We used RT-PCR to determine the quantitative expression levels of *Msx1* and *Msx2*. Fig. 1*C* shows that the expression levels of *Msx1* and *Msx2* in BCs were ~400–500-fold greater than in mBMSCs (**, $p < 0.01$). These genes were up-regulated by 5000-fold in BlCs compared with mBMSCs and 4500-fold in BlCs compared with BCs (****, $p < 0.0001$; Fig. 1*C*, *b* and *d*). Interestingly, endogenous *Msx2* and *Msx1* genes were up-regulated in the transduced MSX1 and MSX2 groups, respectively.

BC cell-surface marker analysis for BlCs and mBMSCs

To confirm BC phenotype for BlCs (mBMSCs as a control group), cells from each group were analyzed by flow cytometry against various surface markers (*i.e.* Sca1, CD31, and Vim). As shown in Fig. 1*D*, the majority of BlCs were positive for Vim (MSX1, 85%; MSX2, 98%), CD31 (MSX1, 45%; MSX2, 35%), and Sca1 (MSX1, 60%; MSX2, 80%), which is comparable with the BC group.

Cell growth, colony-forming unit fibroblast (CFU-F), and cell-cycle analysis

The CFU-F analysis was performed to examine the proliferation patterns of BlCs, BCs, and mBMSCs in semisolid medium. Supplemental Fig. 1*A* shows the colonies and average numbers of colonies per culture dish. The numbers of colonies were 80 ± 5 (mBMSCs), 60 ± 5 (B1Cs), 170 ± 5 (MSX1), and 140 ± 4 (MSX2), as seen in supplemental Fig. 1*C*. The BlCs colonies were significantly longer compared with mBMSCs and BCs (*, $p < 0.05$; supplemental Fig. 1*D*). MTT results indicated that BlCs had a nonsignficantly greater proliferation rate compared with mBMSCs and BCs on day 1. Both MSX1- and MSX2-induced cells had significantly greater proliferation than both BCs and mBMSCs at 3 and 7 days (supplemental Fig. 1*B*). Cell-cycle analysis revealed that the accumulation of BCs and BMSCs in G_0/G_1 phase increased ~2-fold compared with

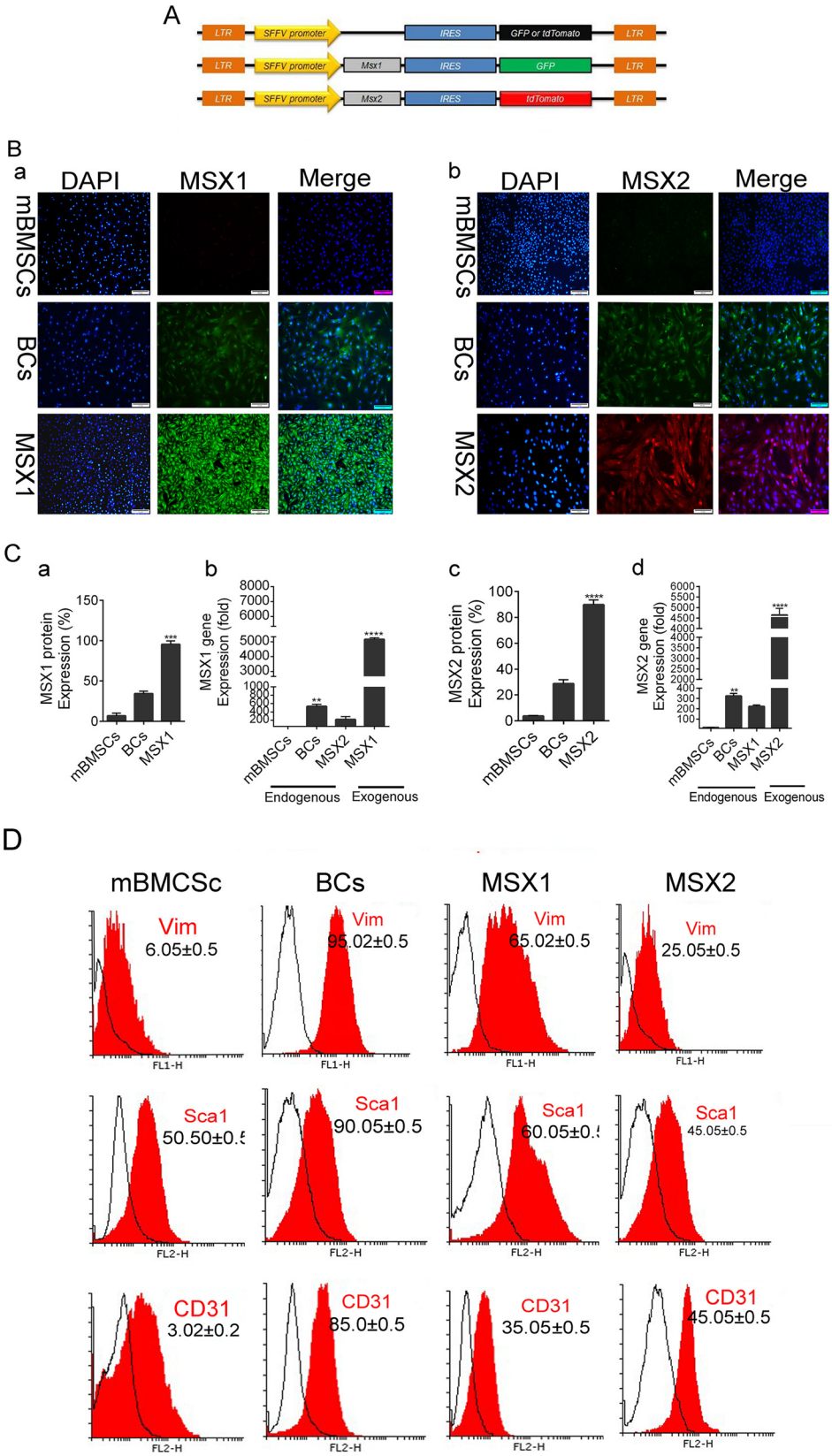

Figure 1. *Msx1* and *Msx2* gene transduction in mBMSCs. *A*, vector map. *Msx1* and *Msx2* were co-expressed by GFP and tdTomato, respectively, to follow *Msx*-positive cells in the same vectors. *B*, the ICC images represent *Msx1* and *Msx2* genes endogenously expressed in mBMSCs and BCs, as well as exogenous *Msx1* (GFP^+) and *Msx2* ($tdTomato^+$) gene expressions in BICs cells (*a* and *b*). *C*, real-time PCR analysis shows the gene expression level of *Msx1* (*b*) and *Msx2* (*d*) in BC, mBMSC, and BIC groups. The histograms represent the percentage of *Msx1* and *Msx2* protein expression levels in BC, mBMSC, and BIC groups (*a* and *c*). *D*, flow cytometry analysis of CD31, Sca1, and Vim cell-surface markers for BICs, BCs, and mBMSCs. *Scale bar*, 50 μm. Data are presented as means ± S.D. (*error bars*). ****, $p < 0.0001$.

MSX1 and MSX2. The percentages of MSX1 and MSX2 in S phase were 32.83 and 40.07%, whereas 13.65 and 14.22% of mBMSCs and BCs were in S phase, respectively (supplemental Fig. 1*E*).

Osteogenic activity

We assessed osteogenic activity of BlCs, BCs, and mBMSCs at various time points (culture days 7, 14, and 21) by alizarin red S staining, alkaline phosphatase (ALP) activity, and qRT-PCR. Alizarin red staining showed that nodule-like aggregates began to form during the first week and increased in abundance toward the end of the third week. There were significantly more mineralized nodules in the BlC (MSX1, MSX2, and MSX1/2) plates compared with BCs and mBMSCs (Fig. 2, *A* and *E*). ALP activity, as an early marker for osteogenic differentiation, was measured after 7, 14, and 21 days of incubation. After 7 days, both *Msx1*- and *Msx2*-transduced cells as well as the MSX1/2 group showed an almost equal increase in ALP activity. ALP activity was significantly reduced in BlCs compared with BCs and mBMSCs. ALP activity was significantly decreased in all of the studied groups on days 14 and 21 (Fig. 2*B*). Fig. 2*C* shows the calcium content of BlC, BC, and mBMSC cultures after 7, 14, and 21 days. The amount of calcium increased over time in all groups. After 14 days, we observed a higher calcium content in BlCs compared with those of BCs and mBMSCs. There was significantly increased calcium content observed between BlC (MSX1, MSX2, and MSX1/2), mBMSC, and BC groups on day 21. Real-time PCR analysis revealed that the expression level of *ColI* (collagen I) as well as *Runx2* and the *Ocn* (osteocalcin) genes was progressively up-regulated within 3 weeks (Fig. 2*D*, *a*–*c*).

Analysis of Msx-related genes

We assessed the expression levels of several major Msx-related genes (*Bmp4*, *Fgf8*, *ki67*, and *K14*) by ICC and RT-PCR before and after gene transduction in mBMSCs as well as BCs. RT-PCR analysis showed that the expression level of *Bmp4* gene increased by 350-fold in MSX1-transduced cells and by 300-fold in MSX2-transduced cells compared with mBMSCs (****, $p < 0.0001$; Fig. 3). The *Fgf8* gene showed significant expression in both the MSX1 (170-fold) and MSX2 (150-fold) groups compared with mBMSCs (Fig. 3*B*, *a* and *b*). ICC analysis indicated that mBMSCs did not express Bmp4 and Fgf8 endogenously, whereas these genes were up-regulated by 80–90% in BlCs (Fig. 3*B*, *b* and *d*). The expression levels of the ectoderm-specific genes keratin 14 (*K14*) and *Ki67* (also known as MKI67) were assessed using ICC. The former is important for nail formation in limb development, and the latter is a cellular marker for proliferation. As shown in Fig. 3*C* (*a*), we detected no endogenous expression of *K14* in mBMSCs, whereas the protein expression level of K14 was significantly up-regulated in *Msx1*- and *Msx2*-transduced cells (80–90%; ****, $p < 0.0001$). In addition, BCs expressed K14 ~20-fold more than mBMSCs (Fig. 3*D* (*a*)). Likewise, ICC results indicated a low expression for Ki67 in mBMSCs (Fig. 3*C* (*b*)) compared with BCs. The expression level of Ki67 protein increased by 90% in the MSX1 group and 80% in the MSX2 group compared with the control group (****, $p < 0.0001$; Fig. 3*D* (*b*)).

Macroscopic evaluation of proximal regeneration

In our digit tip regeneration model, the adult mouse terminal phalanges were proximally amputated to ascertain that the model could not regenerate before injection of the cells (supplemental Fig. 2, *A* and *B*). The wound epidermis formed a scar wound healing response immediately after digit tip amputation at the proximal level of P3 in both the Nrm. Reg and Sham groups (supplemental Fig. 2, *C*–*E*). We observed closure in the epidermis completed in 4–5 days post-amputation (DPA) without any new bone or nail formation. Therefore, we injected the cells 4 DPA, when the scar wound falls off.

Whole-mount digit tip analysis at 6 weeks after the injection (WPI) showed that the epidermal closure occurred in all experimental and control groups. We observed no trace of regeneration in the Nrm. Reg and Sham groups, which was expected (Fig. 4, *B* and *C*). In the BC and mBMSC groups, regeneration of the proximal regions occurred in < 10% of the digit tips. Abnormal bone and nail organ formation with no elongation occurred in both groups (Fig. 4, *D* and *E*, and supplemental Table 2). Surprisingly, > 95% of the digit tips showed full digit tip regeneration, which included both formation and elongation of the bone and nail in the MSX1/2 group (Fig. 4*H* and supplemental Table 2).

In contrast, ~5% of the digit tips fully regenerated in the MSX1 and MSX2 groups. We observed new bone and nail formation in > 50% of samples from both the MSX1 and MSX2 groups (Fig. 4, *F* and *G*, and supplemental Table 2).

To quantify the regenerated bone, we performed whole-mount alizarin red staining to visualize the skeletal patterns to measure the proximal-distal length of each terminal phalanx (30 digits for each group). As illustrated in Fig. 5*A*, the Nrm. Reg and Sham groups formed no nails or new bone (Fig. 5*A*, *b* and *c*). We observed newly formed bone and nail in the mBMSCs and BCs groups (Fig. 5*A*, *d* and *e*), although they had abnormal morphologies with thin nails and short bones. On the other hand, morphological analysis revealed that bone and nail generated up to 50% of the intact group in both the MSX1 and MSX2 groups (Fig. 5, *A* (*f* and *g*) and *B*). There were no remarkable differences in new bone length between the MSX1 and MSX2 groups. The thickness and length of the new nail remarkably increased in MSX1/2 because the length of the newly formed bone was comparable with the intact group (Fig 5, *A* (*h*) and *B*).

Histological analysis of digit tip regeneration

To explore the presence of BlCs in terminal phalange element regeneration, the labeled cells were first traced between the stump bone and wound epidermis position. Ferridex- and GFP-MSX1-labeled cells comprised 15–20% of total cells in digit tip regenerated regions (supplemental Fig. 3). Similarly, BrdU labeling showed the presence of injected cells at the site of injury 6 WPI in all experimental groups (Fig. 6).

Histological analysis showed that epidermal closure occurred in all groups, and the thickness of the epidermis and dermis layer had no significant differences among the groups (Fig. 7). H&E and Masson's trichrome staining results indicated that tissue atrophy occurred in the connective tissue (cartilage,

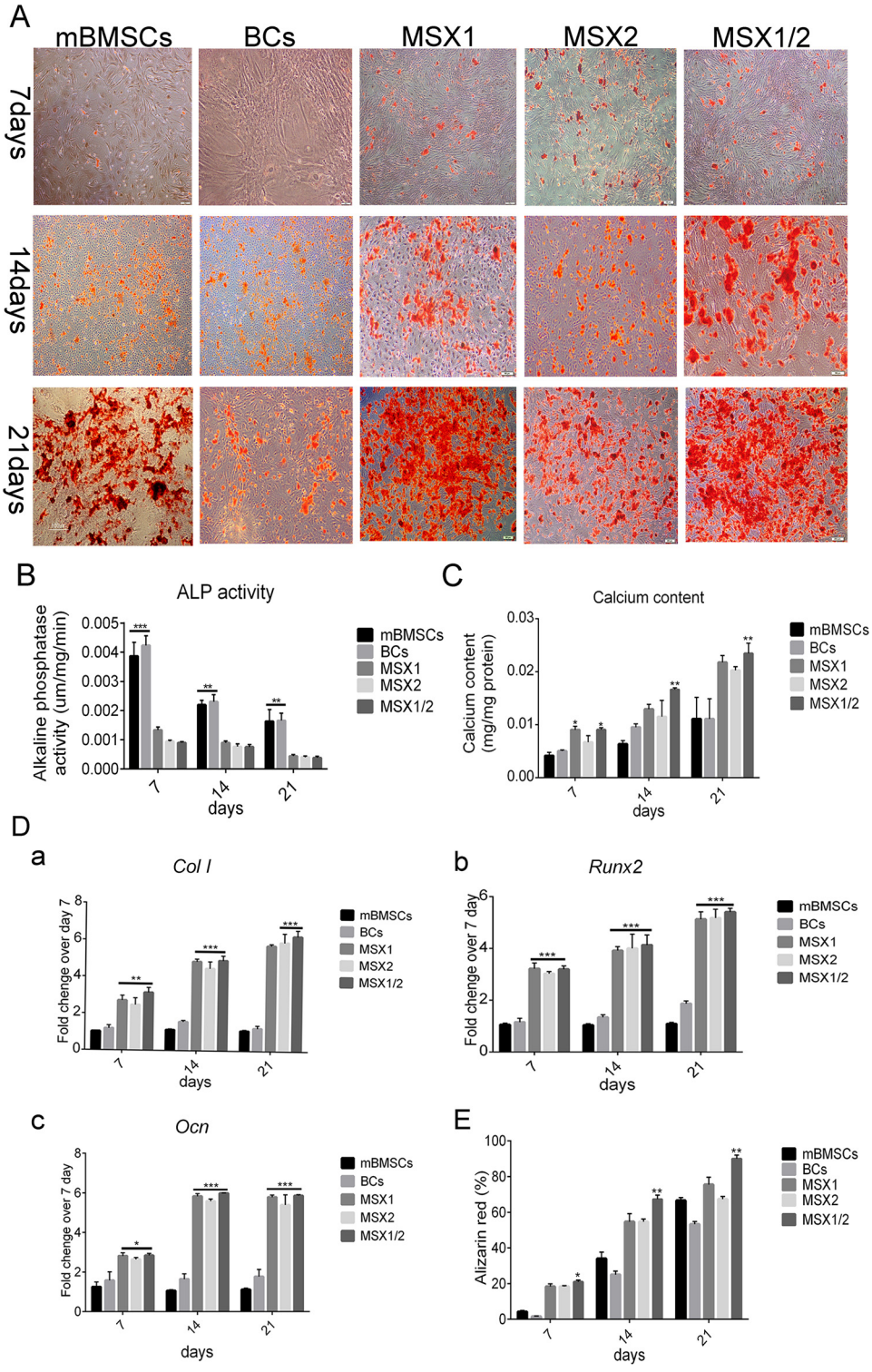

Figure 2. Osteogenic activity. The data represent osteogenic differentiation of BlCs, BCs, and mBMSCs after 7, 14, and 21 days. *A*, nodule-like aggregations increased over time during 3 weeks and showed strong mineralization in all groups. *B*, the histogram shows ALP activity in the BC, mBMSC, MSX1, MSX2, and MSX1/2 groups. *C*, the histogram represents the calcium content in BC, mBMSC, MSX1, MSX2, and MSX1/2 groups. *D*, real-time PCR analysis for *Coll* (*a*), *Runx2* (*b*), and *Ocn* (*c*) genes showed enhanced expression levels in the MSX groups compared with mBMSCs and BCs. *E*, the histogram shows quantitative analysis of mineralized nodules in the BC, mBMSC, MSX1, MSX2, and MSX1/2 groups. Data are presented as means ± S.D. (*error bars*) ($n = 3$). ****, $p < 0.0001$.

nail, and bone stump) in the Nrm. Reg and Sham groups. However, we observed no apoptotic cells or tissue in these groups (Fig. 7, *D* and *H*). In the cell-injected groups, the distal end of the bone stump was elongated and formed a bony cap similar to a bone callus (Fig. 6, *J* and *N*). Specifically, the bone stump showed slight elongation in BCs and mBMSCs, whereas the bone callus was significantly larger in the BlC groups (Fig. 7, *Q–U*, *W*, and *X*). The formed bone callus was spongy in both BCs and mBMSCs. This structure was going to be replaced by a structure similar to compact bone in BlCs. Interestingly, the

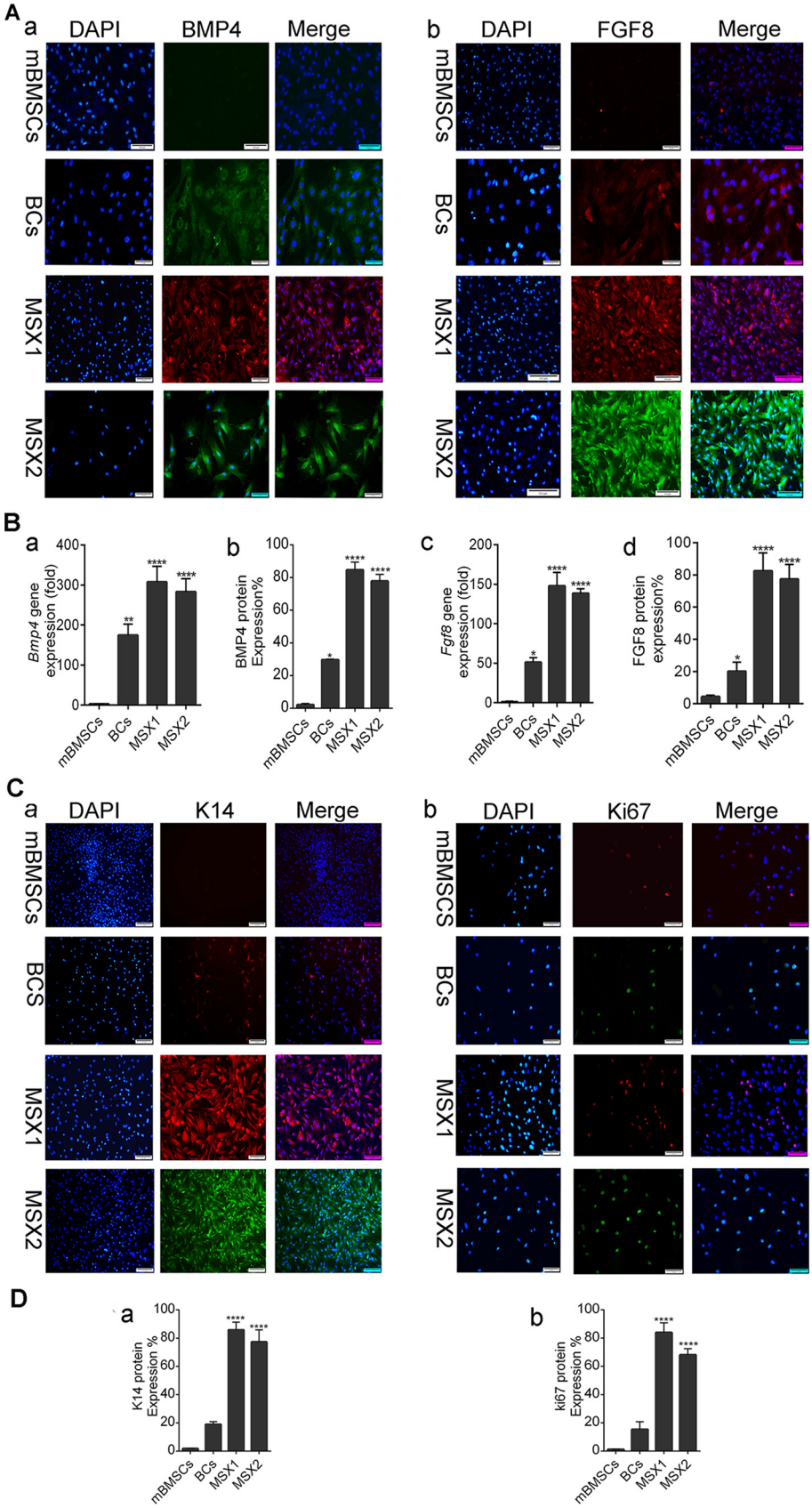
A
a
DAPI
BMP4
Merge
mBMSCs
BCs
MSX1
MSX2
b
DAPI
FGF8
Merge
B
a
Bmp4 gene expression (fold)
b
BMP4 protein Expression%
c
Fgf8 gene expression (fold)
d
FGF8 protein expression%
C
a
DAPI
K14
Merge
b
DAPI
Ki67
Merge
D
a
K14 protein Expression %
b
ki67 protein Expression %

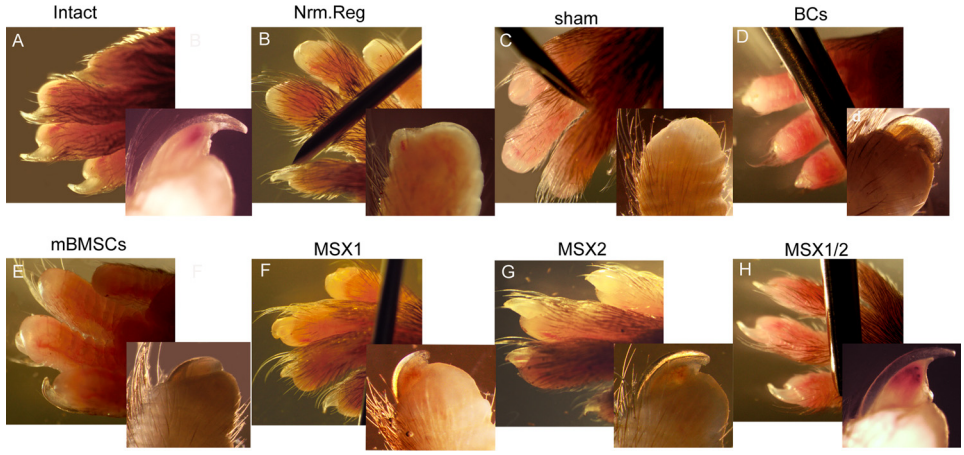

Figure 4. Whole-mount digit tip evaluation at 6 WPI. The images show the macroscopic evaluation of regenerated digit tip of intact (*A*), Nrm. Reg (*B*), sham (*C*), BC (*D*), mBMSC (*E*), MSX1 (*F*), MSX2 (*G*), and MSX1/2 (*H*) groups.

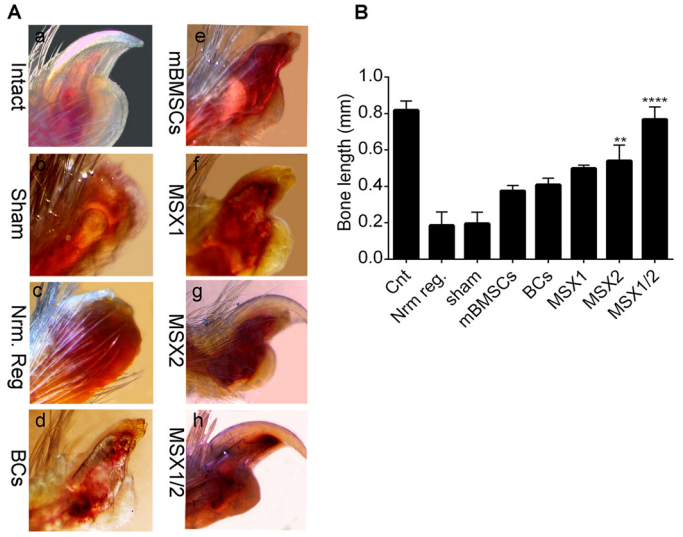

Figure 5. Measurement of bone and nail elongation. *A*, whole-mount alizarin red staining shows bone and nail formation (*a*–*h*). *B*, the histogram shows bone length measurements for all experimental groups. *Error bars*, S.D.

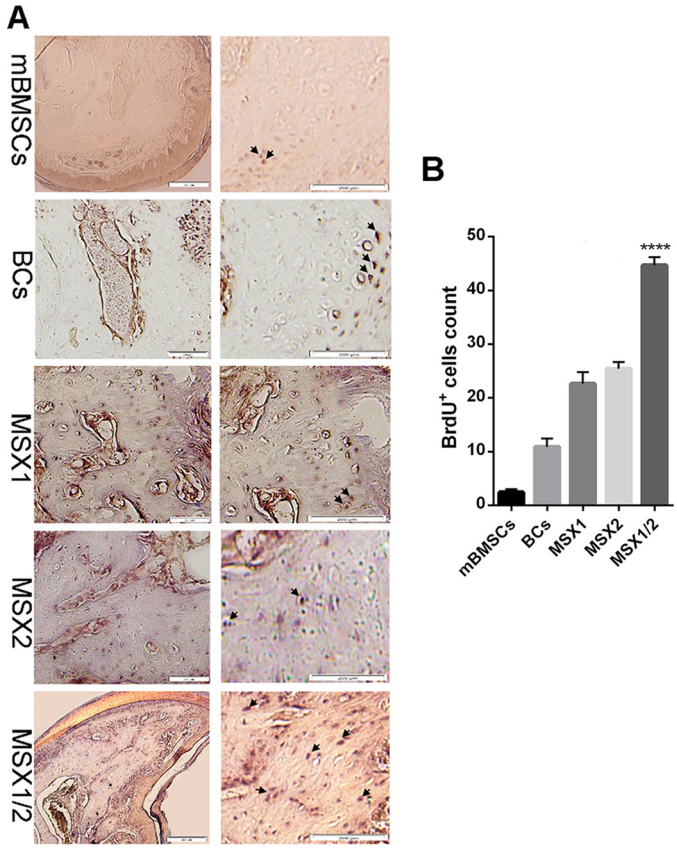

Figure 6. Tracking of BrdU-labeled cells after 6 WPI. *A*, immunohistochemistry illustrates BrdU-labeled cells in mBMSC, BC, MSX1, MSX2 and MSX1/2 groups. *B*, the histogram shows quantitative analysis of $BrdU^+$ cell percentage in bone regenerated regions by ImageJ software in all groups ($n = 3$). The *arrows* show the positions of labeled cells. *Error bars*, S.D.

MSX1/2 groups typically formed bone callus that was greatly similar to that in the intact groups. As illustrated in Fig. 7, we did not observe any distinct bone cavity in both BCs and mBMSCs; however, this cavity was generated in the MSX1 and MSX2 groups. In particular, the bone cavity structure in these groups was similar to that of the intact group. We performed Alcian blue and alizarin red S staining (Al & Al) to determine whether the bone callus-like tissue was bone or cartilage. The results showed that the new bone callus stained a blue color, which indicated cartilage issue in all groups 6 WPI (Fig. 7). Long-term follow-up of the MSX1/2 groups after 10 WPI indicated that the cartilage tissue was replaced by mineralized bone tissue (Fig. 8*A*). IHC analysis for main osteogenic-related markers, including COLI and OCN, also confirmed that newly formed osteoid tissue was matured bone (Fig. 8*B*).

Immunohistochemistry analysis showed that the BC and mBMSC groups expressed relatively low amounts of endogenous MSX1, MSX2, BMP4, and FGF8 proteins (Fig. 9, *A* and

Figure 3. Gene and protein expression analysis of *Bmp4*, *Fgf8*, *K14*, and *Ki67*. *A*, immunostaining of BMP4 (*a*), FGF8 (*b*), and nuclei (DAPI; *blue*). *Left*, merged image with DAPI. *B*, real-time PCR analysis shows the expression level of the *Bmp4* (*a*) and *Fgf8* (*c*) genes in all groups. The histogram shows the amount of BMP4 (*b*) and FGF8 (*d*) protein expressions analyzed by ImageJ software on immunostained slides. *C*, immunostaining of $K14^+$ (*a*) and $Ki67^+$ (*b*). *Left*, shows a merged image with DAPI. *D*, the histogram shows k14 (*a*) and $ki67^+$ (*b*) protein expression level analyzed by ImageJ software. *Scale bar*, 50 μm. Data are presented as means ± S.D. (*error bars*). ****, $p < 0.0001$.

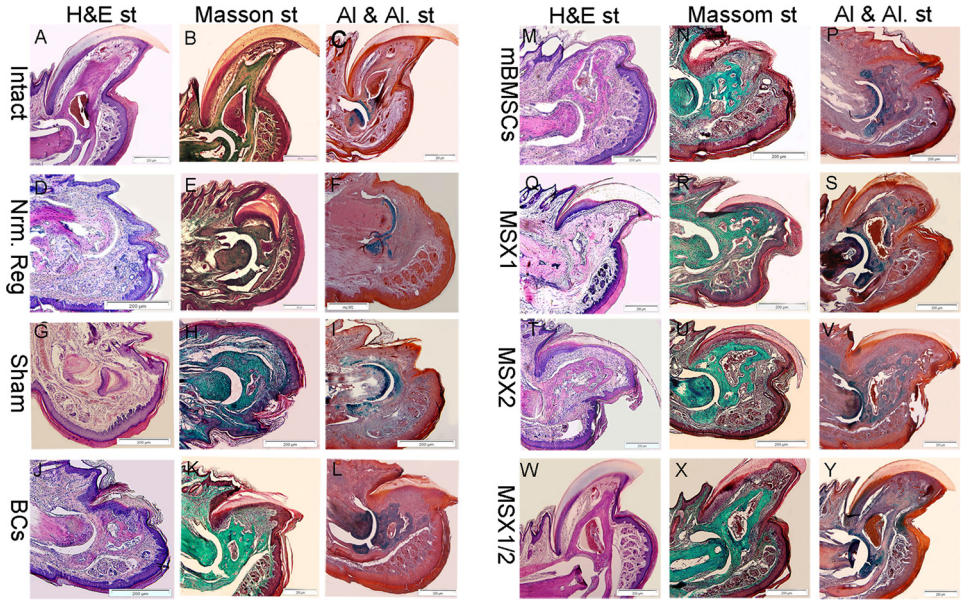

Figure 7. Histological analysis. H&E, Masson's trichrome, Alcian blue, and alizarin red S staining in the intact (*A–C*), Nrm. Reg (*D–F*), sham (*G–I*), BC (*J–L*), mBMSC (*M–O*), MSX1 (*P–R*), MSX2 (*S–U*), and MSX1/2 (*V–Y*) groups. The H&E results showed that no apoptotic cells or tissues were found in any of the groups. Alcian blue-alizarin red S staining indicated that the region containing new bone callus was a *blue color*; we assumed the presence of cartilage tissues that were stained by Alcian blue.

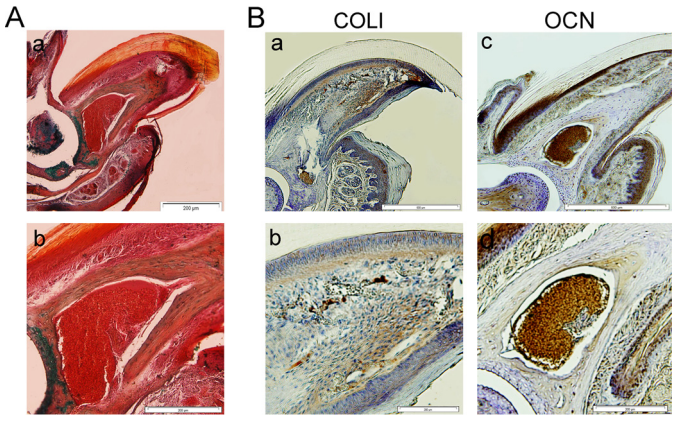

Figure 8. Bone regeneration analysis in MSX1/2 after 10 WPI. *A*, Al & Al staining of MSX1/2 group (*a*, low magnification; *b*, high magnification) 10 WPI that shows the endochondral bone was replaced by mineralized bone. *B*, IHC analysis shows the expression of COLI (*a*, low magnification; *b*, high magnification) and OCN (*c*, low magnification; *d*, high magnification) in mature bone generated in MSX1/2 group after 10 weeks.

B). In contrast, the expression levels of the same markers dramatically increased in the BlC groups, particularly MSX1/2 (Fig. 9, *A* and *B*). These results agreed with the expression profiles of *Msx1*, *Msx2*, *Fgf8,* and *Bmp4* under *in vitro* conditions.

Discussion

Digit tip regeneration in adult mice is restricted to the distal half of the terminal phalangeal element (P3), whereas regeneration fails following amputation through the proximal third of P3 (7) due to lack of BCs and *Msx* genes. *Msx* genes regulate cellular behavior like proliferation and differentiation as well as digit patterning during limb development and regeneration (31). The unavailability of BCs is a major challenge regarding BC therapy. On the other hand, lack of positional information in other cell sources, an exclusive ability of BCs, has hampered the cell-based therapeutic approaches. Therefore, in this study, we have developed a new cell source by overexpression of the *Msx1* and *Msx2* genes in mBMSCs, which created BlCs, after which we explored the regenerative potential these BlCs in proximally amputated digit tips (Fig. 10).

Our ICC and qRT-PCR results showed that *Msx1* and *Msx2* genes were accurately transduced and up-regulated in mBMSCs. Additionally, transduction of exogenous *Msx* genes has resulted in up-regulation of endogenous *Msx2* and *Msx1* in MSX1 and MSX2 cells, respectively. The *Msx2* expression domain has been shown to expand into the *Msx1* domain, and they overlap (7). Therefore, up-regulation of endogenous genes would be expected. Also, overexpression of one of the *Msx* genes may affect expression of the other related genes. A comparison of BlCs and original BCs has confirmed the higher expression levels of the *Bmp4*, *Fgf8*, and *Ki67* genes in BlCs according to ICC results. To determine whether BlCs have the similar characteristics as BCs, we assessed the expression level of specific blastema markers, CD31, Vim, and Sca1, in all groups. Surprisingly, the flow cytometry results confirmed that specific blastema cell-surface markers were significantly expressed in BlCs compared with mBMSCs. These significant differences among mBMSCs, BCs, and BlCs might be attributed to overexpression of *Msx*, which led to a higher proliferation rate and osteogenic activity in the transduced cells. Bmp4 is considered to be a crucial osteogenic marker (32). Its up-regulation in BlCs enhanced osteogenic differentiation capacity compared with mBMSCs and BCs. Likewise, the higher proliferation rate of BlCs occurred because of *Fgf8* and *Ki67* gene up-regulation as proliferation markers. The results of cell-cycle analysis confirmed that S phase in BlCs was longer than mBMSCs and BCs. Of note, the decreased activity of BCs relative to BlCs was most likely related to cellular expansion following several passages *in vitro*.

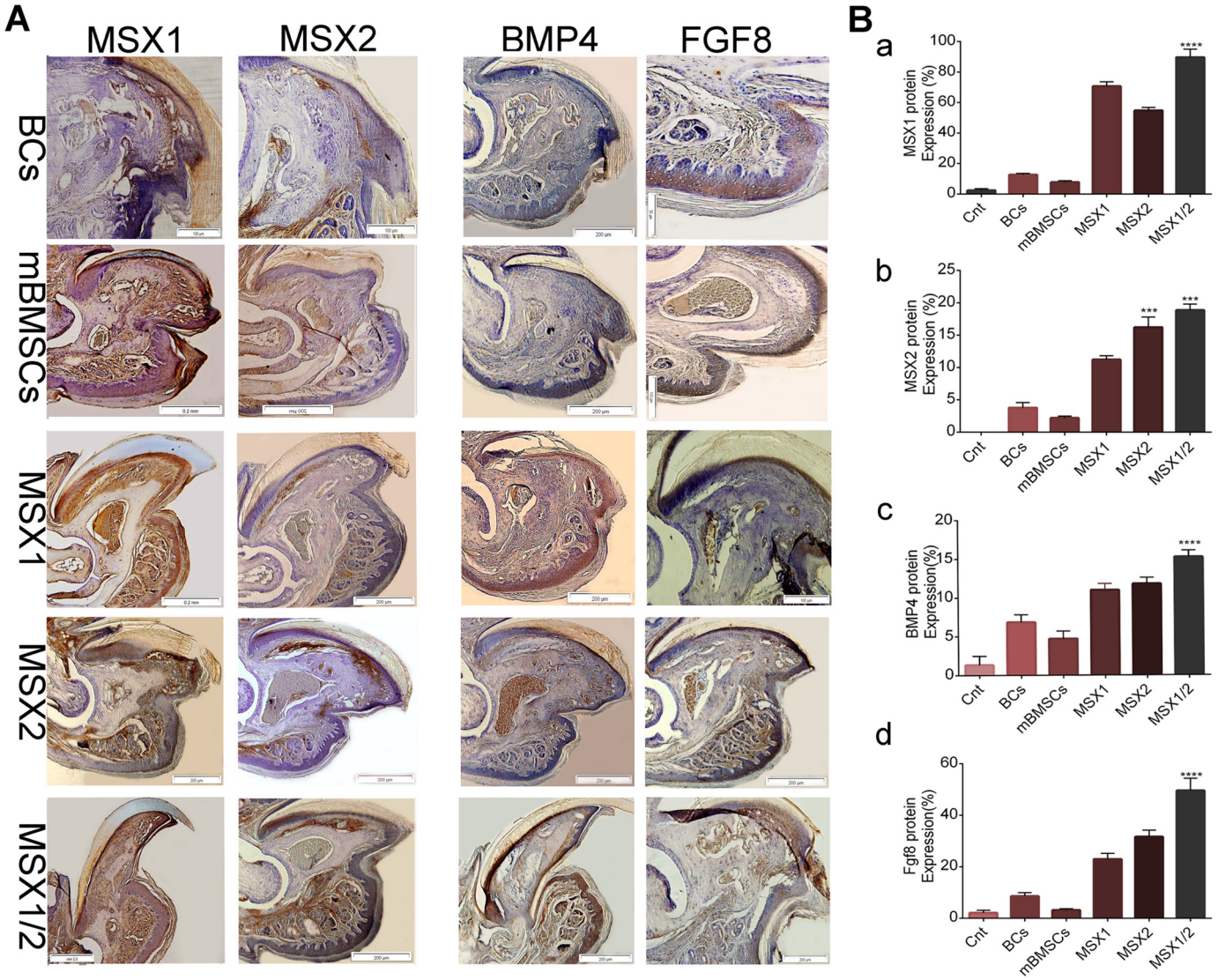

Figure 9. Immunohistochemistry analysis of the MSX1, MSX2, BMP4, and FGF8. *A*, IHC staining shows that MSX1, MSX2, BMP4, and FGF8 were expressed in the BC, mBMSC, MSX1, MSX2, and MSX1/2 groups. *B*, histograms show the percentage of MSX1, MSX2, BMP4, and FGF8 protein expressions in the BCs, mBMSCs, MSX1, MSX2, and MSX1/2 groups (*a–d*). *Error bars*, S.D.

We explored the regenerative capacity of BlCs following transplantation into non-regenerative digit tips of an adult mouse model. In this model, the cartilage tissue of the joint, stump bone, and nail of P3 were preserved, whereas we removed the bone and nail within the bone marrow cavity. Our whole-mount results combined with histological analysis showed a lack of new bone and nail formation as well as tissue atrophy in the non-cell-injected groups (Nrm. Reg and Sham) after 6 WPI, which confirmed that the proximally amputated model was non-regenerative. We observed a significant regenerative response in BlCs, particularly MSX1/2, as indicated by complete nail and bone formation, which was like that of the intact group. We observed abnormal bone and thin nail formation in both the mBMSC and BC groups. These findings showed that the new cell fate of mBMSCs by overexpression of the *Msx* genes efficiently improved regrowth of the amputated digit.

To precisely address how the process of bone formation progresses, we performed Al & Al staining. According to the data, the cell-injected groups induced osteogenesis via an endochondral ossification manner as in a previous study that demonstrated endochondral bone formation in mouse digit tip regeneration (33). The transient cartilage was suggested to be replaced by newly mineralized bone. However, visible changes occurred in the generated bone tissue in terms of volume and histology among the BlCs, mBMSCs, and BCs groups. As expected, injection of BlCs led to regrowth of bone and nail organs, although full regeneration that contained normal bone cavity and compact bone-like was only observed in the MSX1/2 groups after 6 WPI. Long-term follow-up confirmed completion of ossification after 10 WPI in the MSX1/2 group. The presence of very large blood vessels containing blood cells was clearly detected within the regenerated region. Our results are consistent with previous studies that have showed that cells expressing the endothelial markers CD31 and stem cell antigen 1 (Sca1) in the blastema region could differentiate into endothelial progenitor cells and form blood vessels (4). Regenerated bone marrow cavity along with blood vessel formation in BlC

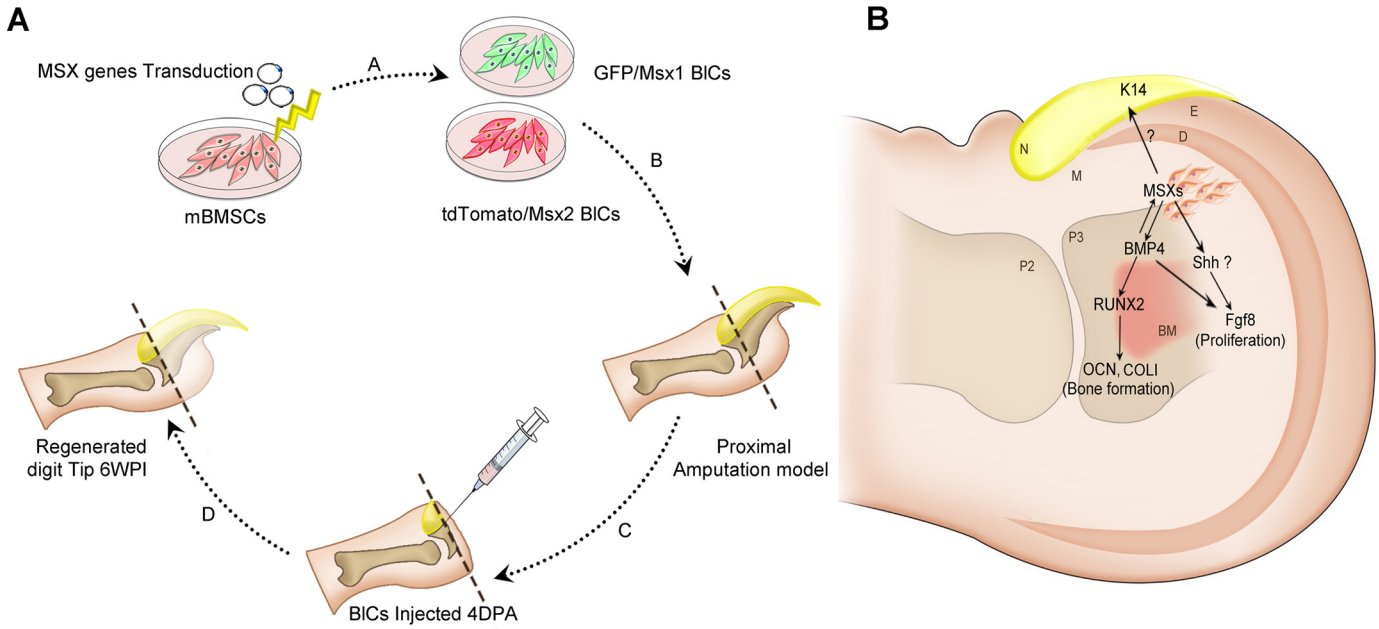

Figure 10. Schematic representation of study design and related mechanism. *A*, mBMSCs are transduced by *Msx1* and *Msx2* genes (*A*). A proximal non-regenerative digit tip model is created (*B*), followed by BlC injection 4 DPA into the models (*C*). Digit tip regeneration has occurred 6 WPI (*D*). *B*, schematic representation of the proposed mechanism by *Msx*-transduced cells on limb regeneration. In this model, *Msx* genes indirectly regulate Runx2 through up-regulation of *Bmp4*, and *Runx2* in turn triggers an osteogenic pathway via *Ocn* and *Coll* expression. *Msx* genes also control the expression of *Fgf8* indirectly either by *Bmp4* or by SHH, which has caused cell proliferation and bone elongation. The up-regulation of *K14* as a consequence of *Msx* genes led to nail formation. *D*, dermis; *M*, mesoderm; *E*, ectoderm; *N*, nail; *P2*, phalanx 2; *P3*, phalanx 3; *BM*, bone marrow.

groups, particularly MSX1/2, compared with BC and mBMSC groups, was most probably related to the increased expression level of CD31 and Sca1 markers after *Msx* transduction. To allocate the improved regeneration to our *Msx*-transduced cells, Ferridex- and BrdU-labeled cells were tracked in the regenerated regions 6 WPI. The presence of labeled cells at the injury site along with expression of *Msx* genes as evidenced by GFP^+ cells demonstrated the contribution of BlCs to digit regeneration.

The expression of *Msx* and its related genes was also shown by IHC results. Interestingly, excellent regeneration occurred in the MSX1, MSX2, and particularly MSX1/2 groups that expressed the highest levels of *Msx1* and *Msx2*. *Msx1* and *Msx2* are greatly expressed in mesenchymal and epithelial cells, respectively (9). Thus, their combination in MSX1/2 caused regeneration of both mesenchymal tissue, such as bone, and epithelial tissue like nail.

It should be taken into consideration that we could not distinguish the expression level of endogenous and exogenous genes due to the lack of a distinct marker *in vivo*. However, the discrepancy of expressed genes between various groups is related to the exogenous gene transduction, which contributes to acceleration of digit regeneration.

The *Msx* genes directly regulate *Bmp4* expression as an essential signaling molecule for bone formation and digit development (13, 34). *Runx2* is also controlled indirectly by *Msx* genes through up-regulation of *Bmp4*. Therefore, enhanced expression level of the *Bmp4* gene in the BlC group compared with mBMSCs and BCs resulted in remarkable bone formation. According to the literature, although essential for bone formation, *Bmp4* expression is not sufficient for full digit tip regeneration. Yu *et al.* (34) have reported improved regeneration but not complete restoration of an injury within the terminal phalangeal element after BMP4 treatment. Exogenous BMP4 partially rescued a digit defect in an *Msx1* mutant in cultured explanted autopods of embryonic day 14.5 neonatal mice. This effect was dose-dependent (7). Therefore, full digit tip regeneration in our study might be related to an enhanced expression level of *Fgf8*, which recovered the ecto-mesodermal interactions as vital events in limb regeneration and development. *Msx* genes control the FGF8 expression indirectly through either the BMP or sonic hedgehog (SHH) signaling pathway (35). The crucial role of *Fgf8* in cell proliferation, as assessed by BrdU labeling, showed significant outgrowth of the regenerating digit in the MSX1/2 group compared with the mBMSC and BC groups. Recently, Satoh *et al.* (36) observed the cooperative inputs of Fgf and Bmp signaling for full-competence limb regeneration in axolotl. Therefore, normal digit regeneration in MSX1/2 might be attributed to direct contribution of BlCs as well as paracrine activity of BlCs through co-overexpression of *Fgf8* and *Bmp4* genes caused by *Msx1* and *Msx2* gene transduction.

We sought to explain why normal nail formation occurred in the BlC groups, whereas we did not observe nail formation in the mBMSC and BC groups. The essential nail-related marker, *K14*, is a well-established marker expressed in mitotically active keratinocytes in the basal epidermis during nail development and regeneration (37). Elevated expression level of *K14* in the BlC groups was believed to be the rationale behind the nail plate formation.

More importantly, *Msx* genes exert their role through the positional information properties on limb patterning (38). Therefore, lack of *Hox* genes (*i.e. Msx1* and *Msx2*) in mBMSCs led to bone formation but without patterning.

Our results demonstrated that overexpression of *Msx1* and *Msx2* in mBMSCs fully regenerated proximally amputated digit tips in adult mice. This study showed that *Msx*-transduced cells exhibited up-regulation of *Bmp4* and *Fgf8* as well as *K14* compared with BCs and mBMSCs. This finding has suggested that ectopic MSCs, which contain exogenous essential genes, activate endogenous signaling pathways and effectively accelerate the regeneration process (Fig. 10*B*). Further experiments are necessary to clearly elucidate the molecular mechanism implicated in up-regulation of the *K14* and *Fgf8* genes related to *Msx.*

Experimental procedures

Isolation and expansion of mBMSCs and BCs

MSCs were isolated from bone marrow of inbred C57LB/6 strain as described previously (39). Isolated cells were cultured in DMEM (Gibco) supplemented with 15% FBS (Gibco), 2 mM L-glutamine (Sigma-Aldrich), and 1% penicillin/streptomycin (Gibco) with medium changes every 3 days. Non-adherent cells were removed by changing the medium, allowing MSCs to proliferate. mBMSCs at passage 3 were used for further experiments.

As we previously reported (30), BCs were isolated from digit tips of 3-day-old newborn C57BL/6 mice, followed by digestion with 0.2% collagenase type I (Gibco) and 0.5% dispase (Sigma-Aldrich). Collected cells were cultured in DMEM supplemented with 15% FBS, 2 mM L-glutamine, and 1% penicillin/streptomycin. Adherent cells were used for subsequent experiments.

Plasmid constructions, virus production, and Msx1 and Msx2 gene transduction

Lentiviral plasmid and virus production was performed according to a protocol described previously (40, 41). Briefly, the cDNAs of *Msx1* and *Msx2* were amplified by PCR and cloned into third generation lentiviral expression vectors. *Msx1* and *Msx2* were cloned into IRES-GFP and IRES-tdTomato viral plasmids, respectively, to form *Msx1*-IRES-GFP and *Msx2*-IRES-tdTomato vectors. The plasmids had similar constitutive promoters, but they differed in co-overexpression marker genes.

To produce lentiviral particles, the HEK293 cells were cultured in fibroblast medium that included G418 (200 μg/ml; Sigma) and nonessential amino acids (10 μl/ml; Life Technologies, Inc.).

Next, 5×10^6 cells were transfected by using Lipofectamine 3000 (Life Technologies) along with the vectors and lentiviral packaging vectors: pMDL, pRev, and pVSVG. Transfection medium was renewed after several hours. The filtered viral supernatant was used for mBMSC transduction along with Polybrene (6 μg/ml; Sigma). Thereafter, transduced cells were expanded for several passages in culture medium. The GFP^+ and $tdTomato^+$ cells were sorted using FACS (BD FACS Aria™ II cell sorter). Sorted cells were expanded for several passages and used for subsequent experiments.

Flow cytometry

To analyze the expression of cell-surface markers, cell-surface antigens were detected using a flow-cytometric technique. Passage-3 BCs and BlCs (mBMSCs as a control group) were first trypsinized, washed, and suspended in PBS. Next, they were incubated with phycoerythrin-conjugated anti-mouse sca1, CD31 (Abcam), and FITC-conjugated anti-mouse Vim (Sigma). As isotype controls, murine FITC-conjugated IgG1 and phycoerythrin-conjugated IgG2b (eBioscience) were substituted for primary antibodies. Data from all samples were collected using a FACScan flow cytometer (BD FACSCaliber, BD Biosciences) and analyzed by Flowing Software version 2.5.

Cell proliferation assay

The MTT assay was performed to evaluate the proliferation of mBMSCs, BCs, and BlCs. Cells were seeded at a density of 5×10^4 cells/ml in triplicate in 96-well tissue culture plates. We added the MTT solution (5 mg/ml) to each well after 1, 3, and 7 days, and the cells were incubated for 3 h at 37 °C. Formazan crystals were dissolved in DMSO, and we measured the intensity of the MTT product at 570 nm using a Thermo Scientific Multiskan™ GO microplate spectrophotometer (Thermo Scientific).

CFU-F assay

We evaluated the colony-forming efficiency of the isolated and transduced cells by the CFU-F assay. Approximately 1000 cells were plated in 60-mm dishes and maintained for 7 days. The colonies were subsequently fixed and stained by crystal violet for 10 min, after which they were counted under an inverted phase-contrast microscope (Olympus, Tokyo, Japan).

Cell-cycle analysis

Cell-cycle analysis was used to quantitatively evaluate cell proliferation. About 1×10^6 cells of mBMSCs, BCs, MSX1, and MSX2 were cultured in the same conditions. After 24–36 h, cells were fixed by 70% ethanol and incubated with RNase for 15 min at 37 °C. PI was used to label DNA content, and the cell-cycle stage of each population was determined by FACS analysis.

Real-time PCR analysis

The gene expression levels of osteogenic-related markers (*ColI*, *Runx2*, and *Ocn*) were examined by qRT-PCR. Briefly, total RNA from cells was extracted using TRI Reagent® (Sigma-Aldrich, T9424). cDNA was produced by the RevertAid First Strand cDNA synthesis kit (Fermentas, K1632) according to the manufacturer's instructions. The expression levels of the target genes were normalized to *GAPDH* as a reference gene. Analysis was performed by the comparative $\Delta\Delta CT$ method. Supplemental Table 1 lists the primers used in this study.

ALP activity

The osteogenic differentiation of BlCs, BCs, and mBMSCs was examined as a function of ALP activity at days 7, 14, and 21. ALP activity was determined with respect to the release of *p*-nitrophenol from *p*-nitrophenyl phosphate substrate using an alkaline phosphatase assay kit (colorimetric; ab83369; Abcam, Cambridge, MA) according to the manufacturer's protocol. Briefly, cells were cultured on 24-well plates at a density of 5×10^4 cells/well. The medium was replaced after 48 h with osteo-

genic medium that contained 0.2 mM ascorbic acid, 10 mM β-glycerophosphate, and 1 nM dexamethasone. For each of the time points, we used lysis buffer to scrape the cell layer from the surface, followed by sonication and centrifugation to collect the cell lysis solution. We added *p*-nitrophenyl phosphate to the cell lysis solution to begin the reaction, which was halted after 60 min by the addition of a stop solution. Optical density was analyzed at 405 nm with a Thermo Scientific Multiskan™ GO microplate spectrophotometer (Thermo Scientific). ALP activity values were normalized with respect to the total protein content obtained from the same cell lysate and expressed as units/μg of total protein. Total protein content was measured using the BCA protein assay kit (EMD Millipore Co., Darmstadt, Germany). The absorbance of the reaction product was measured at 562 nm. The protein concentration was calculated from a standard curve.

Calcium content

Calcium content was measured to evaluate the matrix mineralization ability of BlCs at days 7, 14, and 21 post-induction. The calcium concentration was determined using a calcium colorimetric assay kit (Biovision, Inc.) based on the formation of stable purple-colored complexes with free calcium. The color intensity was detected at 575 nm by a Thermo Scientific Multiskan™ GO microplate spectrophotometer (Thermo Scientific). Color intensity is directly proportional to the calcium concentration of the samples.

ICC and protein expression analysis

We used the immunofluorescent technique to assess the presence of *Msx1* and *Msx2* as main markers of blastema, as well as *Bmp4*, *Fgf8*, *Ki67*, and *K14* as bone differentiation, proliferation, and nail formation markers. Cells were fixed in 4% paraformaldehyde for 20 min and permeabilized with 1% Triton X-100. The fixed cells were blocked with 1% BSA in PBS for 30 min at room temperature and then incubated overnight at 4 °C with primary antibodies that included rat polyclonal anti-mouse BMP4, FGF8, MSX1, MSX2, (Invitrogen), Ki67 (Santa Cruz), and K14 (Biorbyt). Cells were finally incubated with goat anti-rat Alexa Fluor® 488 secondary antibody (1:500; Invitrogen) and goat anti-rat Alexa Fluor® 568 secondary antibody (1:500; Invitrogen) for 60 min at room temperature. Nuclei were counterstained with DAPI (Invitrogen) and analyzed using a fluorescence microscope (Olympus BX51).

Digit tip amputation

C57B/L6 female mice were used in all experiments. Adult mice were anesthetized by ketamine (80 mg/kg body weight) and xylazine (8 mg/kg body weight). Amputations were performed on digits 2, 3, and 4 of the forelimb, at the proximal non-regenerating level. Procedures for care and use of mice were performed in accordance with the standard operating procedures approved by the institutional animal care and ethics Committee of Royan Institute.

Cell labeling by Feridex and BrdU

We used two cell-labeling methods to track cells following transplantation. In the first method, cells were labeled with superparamagnetic iron oxide nanoparticles known as Feridex IV (Sigma) before transplantation. A mixture of Feridex IV (100 μg/ml) and protamine sulfate (45 μg/ml) prepared in serum-free culture medium was directly applied to the attached cells, after which they were incubated for 2 h at 37 °C. Subsequently, 10% FBS, 1% L-glutamine, and 1% penicillin/streptomycin were added to the cells and incubated for 48 h. Cell labeling was performed by incorporation of BrdU using BrdU Detection Kit II (Roche Applied Science) according to the manufacturer's instructions. The labeled cells in the histological sections were tracked using an IX70 inverted microscope (Olympus).

Cell preparation and transplantation

We injected a solution of fibrin glue and medium that contained labeled cells (at a 1:1 ratio) with a final cell concentration of 1×10^5 cells/μl (~$5–7 \times 10^5$ cells/digit) into the amputation wound 4 DPA. Injection was performed using a Hamilton needle under a Stereo Loop (Olympus) between the wound epidermis and the stump of the amputated bone and allowed to hydrate *in situ* before needle removal. The experimental groups consisted of cell-injected groups that included mBMSCs, BCs, MSX1, MSX2, and the combination of MSX1 and MSX2 (MSX1/2, 1:1 ratio). Non-cell-injected groups included an intact digit group (control), Nrm. Reg, and sham (fibrin glue + medium, 1:1 ratio) groups.

Digit harvest and bone length analysis

Mice were euthanized by CO_2 euthanasia chambers, and their digit tips were harvested from both the left and right forelimbs at 6 and 10 WPI. The right digit tip was used for the intact digit group (control). To observe the entire mount digit regeneration, we fixed a random number of digits in 4% PFA overnight at 4 °C. After washing in 1% KOH in H_2O, the digits were incubated serially in 20% glycerol, 1% KOH for 3–6 h; 50% glycerol, 1% KOH for 4–16 h; and 100% glycerol for 2–3 h at room temperature.

To quantify newly formed bone, we measured the proximal-distal length of each terminal phalanx (about 30 random digits for each group). Before staining, the skin was thoroughly removed, and the limbs were fixed in 100% ethanol for 4–6 h. Fixed limbs were then stained with 60% ethanol, 5% acetic acid, 0.015% Alcian blue, 0.005% alizarin red at room temperature for 24 h, followed by washing in 1% KOH, and then transferred into 50% glycerol and stored in 100% glycerol.

Histological analysis

Digits from all experimental groups as well as cell tracking samples were fixed in 4% paraformaldehyde for 24 h at 4 °C, followed by decalcification in Morse's solution (20% formic acid and 10% sodium citrate, pH 7.2) with constant agitation at room temperature for 4 days. Tissues were then embedded in paraffin and cut into 6-μm thickness sections for histological staining.

Prussian blue staining

Ferridex-labeled cells were tracked using Prussian blue staining. Tissue sections from the cell tracking groups were rehydrated and incubated in 2% potassium ferrocyanide (Ajax

Chemical) in 6% hydrochloric acid for 30 min. After washing, nuclear staining was carried out with hematoxylin.

H&E, Masson's trichrome, and Al & Al staining

Samples were first deparaffinized and dehydrated according to standard protocols. Subsequently, sections were stained with Masson's trichrome according to the manufacturer's instructions (Gomori, procedure HT10, Sigma-Aldrich). H&E stains used Gill's hematoxylin to stain nuclei and acidified eosin to counterstain the cytoplasms. To observe the skeletal elements, we stained the samples with alizarin red S and Alcian blue (Al & Al) to detect bone and cartilage, respectively.

Immunohistochemistry

Immunostaining was performed using the following primary antibodies: MSX1 (Abcam), MSX2 (Abcam), BMP4 (eBioscience), and FGF8 (eBioscience). Briefly, the slides were blocked for 30 min in 10% BSA with 2% goat serum, followed by an overnight incubation with primary antibodies at 4 °C. HRP was the secondary antibody at a 1:5000 concentration for 1 h (Invitrogen). The results were visualized by a light microscope (Olympus).

Statistical analysis

Statistical analyses were carried out on data sets that consisted of at least three independent experiments, using an unpaired Student's *t* test that compared two groups: one-way analysis of variance with Tukey's multiple-comparison test, which compared more than two groups, or two-way analysis of variance with Tukey's multiple-comparison test for nonparametric results with GraphPad Prism software (GraphPad, La Jolla, CA). All data are expressed as the mean ± S.D. *, $p < 0.05$; **, $p < 0.01$; ***, $p < 0.001$; ****, $p < 0.0001$.

Author contributions—L. T. designed, performed, and analyzed the experiments shown in all figures and wrote the paper. M. H. designed and constructed vectors for transduction and expression of *Msx* genes. F. A. S. provided the quantitative PCR technical assay and contributed to the data analysis of quantitative PCR. L. S. provided technical assistance and cell injection. S. H. edited the paper and contributed to the preparation of the figures. N. A. coordinated the study. M. B. E. conceived and coordinated the study, provided technical assistance, and wrote the paper. All authors reviewed the results and approved the final version of the manuscript.

References

1. Suzuki, M., Yakushiji, N., Nakada, Y., Satoh, A., Ide, H., and Tamura, K. (2006) Limb regeneration in *Xenopus laevis* froglet. *ScientificWorldJournal* **6,** 26–37
2. Muller, T. L., Ngo-Muller, V., Reginelli, A., Taylor, G., Anderson, R., and Muneoka, K. (1999) Regeneration in higher vertebrates: limb buds and digit tips. *Semin. Cell Dev. Biol.* **10,** 405–413
3. Kragl, M., Knapp, D., Nacu, E., Khattak, S., Maden, M., Epperlein, H. H., and Tanaka, E. M. (2009) Cells keep a memory of their tissue origin during axolotl limb regeneration. *Nature* **460,** 60–65
4. Fernando, W. A., Leininger, E., Simkin, J., Li, N., Malcom, C. A., Sathyamoorthi, S., Han, M., and Muneoka, K. (2011) Wound healing and blastema formation in regenerating digit tips of adult mice. *Dev. Biol.* **350,** 301–310
5. Allan, C. H., Fleckman, P., Fernandes, R. J., Hager, B., James, J., Wisecarver, Z., Satterstrom, F. K., Gutierrez, A., Norman, A., Pirrone, A., Underwood, R. A., Rubin, B. P., Zhang, M., Ramay, H. R., and Clark, J. M. (2006) Tissue response and Msx1 expression after human fetal digit tip amputation *in vitro*. *Wound Repair Regen.* **14,** 398–404
6. Carlson, M. R., Bryant, S. V., and Gardiner, D. M. (1998) Expression of Msx-2 during development, regeneration, and wound healing in axolotl limbs. *J. Exp. Zool.* **282,** 715–723
7. Han, M., Yang, X., Farrington, J. E., and Muneoka, K. (2003) Digit regeneration is regulated by Msx1 and BMP4 in fetal mice. *Development* **130,** 5123–5132
8. Wang, Y., and Sassoon, D. (1995) Ectoderm-mesenchyme and mesenchyme-mesenchyme interactions regulate Msx-1 expression and cellular differentiation in the murine limb bud. *Dev. Biol.* **168,** 374–382
9. Bensoussan-Trigano, V., Lallemand, Y., Saint Cloment, C., and Robert, B. (2011) Msx1 and Msx2 in limb mesenchyme modulate digit number and identity. *Dev. Dyn.* **240,** 1190–1202
10. Barker, D. M., and Beck, C. W. (2009) Overexpression of the transcription factor Msx1 is insufficient to drive complete regeneration of refractory stage *Xenopus laevis* hindlimbs. *Dev. Dyn.* **238,** 1366–1378
11. Han, M. J., An, J. Y., and Kim, W. S. (2001) Expression patterns of Fgf-8 during development and limb regeneration of the axolotl. *Dev. Dyn.* **220,** 40–48
12. Ide, H. (2012) Bone pattern formation in mouse limbs after amputation at the forearm level. *Dev. Dyn.* **241,** 435–441
13. Yu, L., Han, M., Yan, M., Lee, J., and Muneoka, K. (2012) BMP2 induces segment-specific skeletal regeneration from digit and limb amputations by establishing a new endochondral ossification center. *Dev. Biol.* **372,** 263–273
14. Simon, H. G., and Tabin, C. J. (1993) Analysis of Hox-4.5 and Hox-3.6 expression during newt limb regeneration: differential regulation of paralogous Hox genes suggest different roles for members of different Hox clusters. *Development* **117,** 1397–1407
15. Rao, N., Song, F., Jhamb, D., Wang, M., Milner, D. J., Price, N. M., Belecky-Adams, T. L., Palakal, M. J., Cameron, J. A., Li, B., Chen, X., and Stocum, D. L. (2014) Proteomic analysis of fibroblastema formation in regenerating hind limbs of *Xenopus laevis* froglets and comparison to axolotl. *BMC Dev. Biol.* **14,** 32 25063185
16. Stoltz, J. F., de Isla, N., Li, Y. P., Bensoussan, D., Zhang, L., Huselstein, C., Chen, Y., Decot, V., Magdalou, J., Li, N., Reppel, L., and He, Y. (2015) Stem cells and regenerative medicine: myth or reality of the 21th century. *Stem Cells Int.* **2015,** 734731
17. Vojnits, K., Pan, H., Mu, X., and Li, Y. (2015) Characterization of an injury induced population of muscle-derived stem cell-like cells. *Sci. Rep.* **5,** 17355
18. Bajek, A., Gurtowska, N., Olkowska, J., Kazmierski, L., Maj, M., and Drewa, T. (2016) Adipose-derived stem cells as a tool in cell-based therapies. *Arch. Immunol. Ther. Exp.* **64,** 443–454
19. Wu, X., Wang, W., Meng, C., Yang, S., Duan, D., Xu, W., Liu, X., Tang, M., and Wang, H. (2013) Regulation of differentiation in trabecular bone-derived mesenchymal stem cells by T cell activation and inflammation. *Oncol. Rep.* **30,** 2211–2219
20. Cai, T. Y., Zhu, W., Chen, X. S., Zhou, S. Y., Jia, L. S., and Sun, Y. Q. (2013) Fibroblast growth factor 2 induces mesenchymal stem cells to differentiate into tenocytes through the MAPK pathway. *Mol. Med. Rep.* **8,** 1323–1328
21. Toma, C., Pittenger, M. F., Cahill, K. S., Byrne, B. J., and Kessler, P. D. (2002) Human mesenchymal stem cells differentiate to a cardiomyocyte phenotype in the adult murine heart. *Circulation* **105,** 93–98
22. Maleki, M., Ghanbarvand, F., Reza Behvarz, M., Ejtemaei, M., and Ghadirkhomi, E. (2014) Comparison of mesenchymal stem cell markers in multiple human adult stem cells. *Int. J. Stem. Cells* **7,** 118–126
23. Ono, I., Yamashita, T., Hida, T., Jin, H. Y., Ito, Y., Hamada, H., Akasaka, Y., Ishii, T., and Jimbow, K. (2004) Combined administration of basic fibroblast growth factor protein and the hepatocyte growth factor gene enhances the regeneration of dermis in acute incisional wounds. *Wound Repair Regen.* **12,** 67–79
24. Shah, M., Foreman, D. M., and Ferguson, M. W. (1995) Neutralisation of TGF-β1 and TGF-β2 or exogenous addition of TGF-β3 to cutaneous rat wounds reduces scarring. *J. Cell Sci.* **108**, 985–1002

25. Müller, I., Kordowich, S., Holzwarth, C., Isensee, G., Lang, P., Neunhoeffer, F., Dominici, M., Greil, J., and Handgretinger, R. (2008) Application of multipotent mesenchymal stromal cells in pediatric patients following allogeneic stem cell transplantation. *Blood Cells Mol. Dis.* **40,** 25–32
26. Klinker, M. W., and Wei, C. H. (2015) Mesenchymal stem cells in the treatment of inflammatory and autoimmune diseases in experimental animal models. *World J. Stem Cells* **7,** 556–567
27. Penfornis, P., and Pochampally, R. (2011) Isolation and expansion of mesenchymal stem cells/multipotential stromal cells from human bone marrow. *Methods Mol. Biol.* **698,** 11–21
28. Masaki, H., and Ide, H. (2007) Regeneration potency of mouse limbs. *Dev. Growth Differ.* **49,** 89–98
29. Rinkevich, Y., Lindau, P., Ueno, H., Longaker, M. T., and Weissman, I. L. (2011) Germ-layer and lineage-restricted stem/progenitors regenerate the mouse digit tip. *Nature* **476,** 409–413
30. Taghiyar, L., Hosseini, S., Hesaraki, M., Sayahpour, F. A., Aghdami, N., and Baghaban Eslaminejad, M. (2017) Isolation, characterization and osteogenic potential of mouse digit tip blastema cells in comparison with bone marrow-derived mesenchymal stem cells *in vitro*. *Cell (Yakhteh*), in press
31. Hu, G., Lee, H., Price, S. M., Shen, M. M., and Abate-Shen, C. (2001) Msx homeobox genes inhibit differentiation through upregulation of cyclin D1. *Development* **128,** 2373–2384
32. Bandyopadhyay, A., Tsuji, K., Cox, K., Harfe, B. D., Rosen, V., and Tabin, C. J. (2006) Genetic analysis of the roles of BMP2, BMP4, and BMP7 in limb patterning and skeletogenesis. *PLoS Genet.* **2,** e216
33. Lehoczky, J. A., Robert, B., and Tabin, C. J. (2011) Mouse digit tip regeneration is mediated by fate-restricted progenitor cells. *Proc. Natl. Acad. Sci. U.S.A.* **108,** 20609–20614
34. Yu, L., Han, M., Yan, M., Lee, E. C., Lee, J., and Muneoka, K. (2010) BMP signaling induces digit regeneration in neonatal mice. *Development* **137,** 551–559
35. Nacu, E., Gromberg, E., Oliveira, C. R., Drechsel, D., and Tanaka, E. M. (2016) FGF8 and SHH substitute for anterior-posterior tissue interactions to induce limb regeneration. *Nature* **533,** 407–510
36. Satoh, A., Makanae, A., Nishimoto, Y., and Mitogawa, K. (2016) FGF and BMP derived from dorsal root ganglia regulate blastema induction in limb regeneration in *Ambystoma mexicanum*. *Dev. Biol.* **417,** 114–125
37. Coulombe, P. A., Kopan, R., and Fuchs, E. (1989) Expression of keratin K14 in the epidermis and hair follicle: insights into complex programs of differentiation. *J. Cell Biol.* **109,** 2295–2312
38. Pizette, S., Abate-Shen, C., and Niswander, L. (2001) BMP controls proximodistal outgrowth, via induction of the apical ectodermal ridge, and dorsoventral patterning in the vertebrate limb. *Development* **128,** 4463–4474
39. Eslaminejad, M. B., Nikmahzar, A., Taghiyar, L., Nadri, S., and Massumi, M. (2006) Murine mesenchymal stem cells isolated by low density primary culture system. *Dev. Growth Differ.* **48,** 361–370
40. Dehghan, S., Hesaraki, M., Soleimani, M., Mirnajafi-Zadeh, J., Fathollahi, Y., and Javan, M. (2016) Oct4 transcription factor in conjunction with valproic acid accelerates myelin repair in demyelinated optic chiasm in mice. *Neuroscience* **318,** 178–189
41. Reiser, J. (2000) Production and concentration of pseudotyped HIV-1-based gene transfer vectors. *Gene. Ther.* **7,** 910–913